Waste Isolation Pilot Plant

Compliance Certification Application

Reference 52

Beauheim, R.L., W.R. Wawersik, and R.M. Roberts, 1993.
Coupled Permeability and Hydrofracture Test to Assess the Waste-Containment Properties of Fractured Anhydrite, International Journal of Rock Mechanics and Mining Sciences & Geomechanics Abstracts, Vol. 30, No. 7, 1159-1163. (CONF930644, ISSN:0148-9062)

Submitted in accordance with 40 CFR §194.13, Submission of Reference Materials.

SAND93-0639J

COUPLED PERMEABILITY AND HYDROFRACTURE TESTS TO ASSESS THE WASTE-CONTAINMENT PROPERTIES OF FRACTURED ANHYDRITE

R.L. Beauheim and W.R. Wawersik
Geoscience and Geotechnology Center 6100
Sandia National Laboratories
Albuquerque, NM 87185

R.M. Roberts
INTERA Inc.
1650 University Blvd. NE, Suite 300
Albuquerque, NM 87102

INTRODUCTION

Combined permeability and hydrofracturing tests are being conducted at the Waste Isolation Pilot Plant (WIPP) site near Carlsbad, New Mexico to evaluate how a polyhalitic-anhydrite interbed, MB139, will respond to high gas pressures generated within the repository. Two mechanisms that might limit the gas-pressure buildup in disposal rooms are being evaluated. First, fracture development in MB139 and an attendant increase in permeability might allow gas to flow away from the disposal rooms. Second, the interbed gas-storage capacity might be increased either by the interconnection of pre-existing matrix and fracture porosity, or by the creation of new fracture porosity. Toward this end, the combined hydraulic fracturing and hydrologic tests address five questions: (1) What are the pressures needed to initiate and extend interbed fractures? (2) Will fracturing occur by reopening and interconnecting pre-existing fractures and/or by forming discrete new fractures? (3) Is the combination of the *in situ* stress state and pre-existing weakness planes in the interbed such that fracturing will be contained within MB139, or might newly developed fractures break out of MB139? (4) How does fracture development change interbed permeability and storage capacity? (5) Are the post-fracturing permeability and storage capacity of MB 139 constant, or are they dependent on pressure?

All papers must include the following statement:

This work performed at Sandia National Laboratories supported by the U.S. Department of Energy under contract DE-AC04-76DP00789.

SITE DESCRIPTION

MB139 is a structurally complex, approximately 1-m-thick polyhalitic-anhydrite layer with halite inclusions separated above and below from bounding rock-salt beds by undulatory, clay-rich zones [1]. The bottom third of MB139, and to a lesser degree the top third, contain closely spaced, fully or partially healed, subhorizontal fractures (Figure 1). These fractures may not be horizontally pervasive on the scale of the repository. Test holes were drilled into the floor of a 5.5-m-wide, 30-m-long room (Room C1) approximately 7 m above the upper contact of MB139 (Figure 2). A trial test hole, C1X10, was located at the room entrance to evaluate the local MB139 stratigraphy, formation pore pressure, and test procedures. A second test hole, C1X05, was drilled at the end of Room C1, as far as possible from other excavations that might have altered the virgin ground conditions. Observation holes were drilled around both test holes at distances between 3 and 10 m from the test holes (Figure 2). One observation hole (C1H06) was slanted to intersect MB139 under the nearest pillar. The observation holes provided stratigraphic details, pressure measurements, and post-test data on flow and fracture paths.

EXPERIMENTS

The experimental sequence in each test hole consisted of an initial pressure-buildup period to establish the formation pore pressure, a pre-frac permeability test, hydrofracturing, and post-frac permeability tests (Figure 3). The post-frac tests included both constant-pressure injection and withdrawal to evaluate post-frac permeability under different pressure conditions. The test intervals spanned all of MB139 with the exception of the top and bottom argillaceous contact zones. The intervals were isolated with a conventional straddle-packer system with two supply lines for independent monitoring and control of packer and test-interval pressures. Fluid and pressure buildup in the bottom of the borehole below the lower packer could be monitored through a central vent line.

All tests were performed with Chevron Mineral Seal Oil 38 (viscosity 2.2 cp at 40°C) with 5% by volume fluorescent dye. Packer pressures were maintained constant between 1.4 and 2.8 MPa above the interval pressures. The flow rate during hydraulic fracturing was 5.7 L/min with a maximum fluid injection of 11.3 L per pressure cycle. Fluid injection and backflow, as well as flow rates during flow tests, were measured and controlled by a combination of a flow meter and differential-pressure measurements with respect to a reference fluid column. Fracturing and flow measurements were complemented by pre- and post-test borehole television observations.

PRE-TEST SIMULATIONS

Before testing began, numerical simulations were performed assuming uniform, radial-flow conditions to optimize test durations and to ensure that fracture-induced changes in interbed permeability could be distinguished and measured. The pre-test calculations also aided in establishing the layout of observation holes. An estimated pre-test permeability of 10^{-19} m^2 resulted in predicted flow rates of approximately 20 mL/day under a 1.6-MPa driving pressure, mandating careful pre-test evaluation of system leaks and packer deformability. Figure 4 shows a comparison of predicted flow volumes from a constant-pressure injection test before fracturing and after fracturing, for fractures of two different extents.

RESULTS OF HYDRAULIC-FRACTURING TESTS

The pore pressures at C1X10 and C1X05 were 7.4 and 9.6 MPa, respectively, when the hydraulic-fracturing tests began. Substantial brine and gas inflow during the few hours between drilling and packer installation in C1X10 suggested the existence of one or more at least partially open fractures near the entrance to Room C1. As confirmation, hydraulic fracturing in C1X10 exhibited only a 1.4-MPa difference between the primary breakdown pressure and the fracture-extension pressure before shut-in. At C1X05, in contrast, little brine inflow, a slow

equilibration with the formation pore pressure, and a substantially higher primary breakdown signature during hydraulic fracturing (Figure 5) indicated that the rock at that location was initially competent. A partial listing of the pressure data of both hydraulic-fracturing tests is given in Table 1. The observed instantaneous shut-in pressures agree well with calculated vertical stresses of 9.8 and 13.0 MPa at the locations of C1X10 and C1X05, respectively [2].

Post-frac television scans, coring operations, and pressure responses in observation holes showed that hydraulic fracturing opened one or more of the pre-existing, partially or fully healed, subhorizontal fractures near the bottom of MB139. The instantaneous shut-in pressures in Table 1 must, therefore, be equal to the vertical stresses, normal to the hydraulically driven fractures. The vertical stress normal to fractures in borehole C1X10 was approximately 4 MPa lower than the vertical stress in borehole C1X05, while the vertical stress at C1X05 approached the vertical virgin *in situ* stress of 14.9 MPa at the depth of the repository [3]. These results imply that measurements at C1X05 are more representative of the response of undisturbed MB139 than data gathered at C1X10 near the room entrance. The difference in pore pressures between C1X10 and C1X05 may be related to excavation-induced fracturing around C1X10 opening new porosity, creating a permeable, depressurized region. Similar excavation-related fracturing did not take place at the location of C1X05 because the vertical (resisting) stress was greater. The pressures between the two holes may not have equilibrated during the time since the room was excavated because of the low permeability of MB139 or because of continuing excavation-related fracture opening near the entrance to the room. Alternatively, the continuing existence of a several-MPa pressure difference over the 25-m distance between C1X10 and C1X05 may imply that an active local flow system exists, with fluid from C1X10 and C1X05 flowing toward some other, lower pressure location beneath the repository.

It is not yet clear whether hydraulically, i.e., pressure-induced, fracturing in MB139 is restricted to discrete fracture formation, or whether fracturing can extend to multiple fracturing

and fracture branching, perhaps favored by closely spaced, partially interconnected, pre-existing weakness planes. Core taken from borehole C1H07 suggests the former. On the other hand, after pressures at C1H05 and C1H06 had initially begun to increase during constant-pressure injection tests in both C1X10 and C1X05, they showed temporary stabilizations or slight decreases before resuming their increase. These observations suggest pressure interference between several adjacent fractures or connections of fractures that slowly propagated until they met with time. Considering the inhomogeneity of MB139, multiple fracturing and/or fracture branching appears likely. Additional evidence for multiple fracturing was provided by the video observation of dyed fracture fluid emanating from still tight, healed subhorizontal fractures in the top third of MB139 in observation holes C1H05 and C1H06 in addition to the fracture fluid observed in the lower third of MB139 in core from those holes.

Approximately 67% (12L) of the oil pumped into MB139 was retained in newly created storage space associated with a residual fracture aperture at the end of the hydraulic-fracturing tests in the near-virgin area around C1X05. If all of this fluid were held in a single fracture extending under all of Room C1 from the test hole C1X05 to the location of the observation hole C1H07, then the mean residual fracture aperture would be about 0.2 mm. The residual aperture results from a mismatch of adjacent fracture surfaces, preventing complete closure once the hydraulic-fracturing pressure was reduced.

RESULTS OF PERMEABILITY TESTS

Borehole C1X10

Hydraulic fracturing results and rapid gas and brine inflow immediately after borehole C1X10 was drilled suggested a locally high pre-frac permeability in MB139. The volume of fluid injected (7.8 L) during the pre-frac constant-pressure injection test was approximately three

orders of magnitude greater than simulations had predicted assuming a permeability of approximately 10^{-19} m^2. Therefore, the permeability at C1X10 may have been on the order of 10^{-16} m^2. The pre- and post-frac constant-pressure injection and withdrawal tests in C1X10 were conducted at driving pressure differentials of about 1.6 MPa above and below the formation pore pressure existing at the start of each test. The resulting flow rates are shown in Figure 6. The highest flow rates occurred during post-frac constant-pressure injection at 9.1 MPa. The late-time flow rates during the post-frac constant-pressure withdrawal test at 6.5 MPa were intermediate between those observed during the pre-frac injection test at 8.3 MPa and the post-frac injection test. The relative flow rates observed indicate that hydrofracturing opened one or more pre-existing fractures, creating a net increase in interbed permeability but also leaving that permeability sensitive to the fluid pressure in the fracture.

The pre-frac constant-pressure injection test revealed the existence of a locally conductive region within a less conductive domain. The decline in the flow rate with time was matched using an analytical solution representing flow through a medium having a non-Euclidean spatial flow dimension of -0.25 (Figure 6). A sublinear flow dimension of -0.25 indicates that the fracture conductance (permeability-area product) decreases with the -1.25 power of distance from the test hole [4]. These results appear to reflect the aperture variations of relatively short fractures from mouth to tip. They are qualitatively consistent with a model for the maximum and mean apertures of radial hydraulic fractures, $d \propto R^{1/4}$ [5] where d is aperture and R is fracture radius. The sublinear flow dimension interpreted from the flow-rate data implies that interpretation of the pressure-falloff data using standard radial-flow models would provide unreliable estimations of permeability. In fact, attempts at matching both the flow and pressure-falloff data using a radial-flow model were unsuccessful.

The flow rate during the post-frac constant-pressure injection test was higher than before hydraulic fracturing but continued to exhibit the spatial flow dimension of -0.25. The flow

dimension during constant-pressure withdrawal at 6.5 MPa increased to 0.15 (Figure 6), perhaps resulting from partial fracture closure and attendant reduction in fracture conductance near the test borehole.

The pressures in C1H05 and C1H06 stabilized within 3 hr during the post-frac injection test but not at all during the 6-hr withdrawal test. Stable pressures at the observation holes suggest that they had effectively become part of the test hole and that fluid flow from the test hole C1X10 was controlled by the interbed properties beyond C1H05 and C1H06. Hence, fractures between C1X10 and the observation holes must have been sufficiently open to provide negligible resistance to flow. Continuously decreasing pressures in C1H05 and C1H06 during the withdrawal test suggest increasing flow resistance as the pressure-sensitive fracture closed.

Borehole C1X05

The pre-frac permeability test in C1X05 indicated a permeability of MB139 of approximately 10^{-20} m^2. The interbed at this location appeared to be relatively undisturbed as suggested also by the high primary breakdown pressure during hydraulic fracturing (Figure 4). Not surprisingly, therefore, the difference between pre-frac and post-frac hydraulic properties at C1X05 was more pronounced than at C1X10.

Figure 6 shows the flow rates for the pre- and post-frac constant-pressure injection tests in C1X05. For pressure differentials of approximately 1 MPa, the post-frac flow rates were over two orders of magnitude greater than the pre-frac rates. A 2.3-MPa pressure differential caused the flow rates to increase by a factor of 10^5 compared with pre-test conditions. Substantially lower flow rates during the post-frac withdrawal test confirm that the permeability of newly created or opened fractures is highly, and non-linearly, dependent on fracture aperture and fluid pressure within the fracture. Such behavior is consistent with a cubic law approximation relating fracture permeability to aperture.

During both the pre- and post-frac constant-pressure injection tests, the flow rates declined rapidly for 1 to 2 hr before settling into an apparent radial-flow regime (having a spatial flow dimension of 2) (Figure 6). However, late in the post-frac test, the flow rate appeared to stabilize as if steady-state conditions had been reached. If the hydraulic properties of the system did not change, this could only occur if a constant-pressure boundary had been reached, which is unlikely. The stabilization of the flow rate may, therefore, represent a continuing change in fracture properties such as permeability, storage capacity, and/or extent.

Additional evidence for changes in the fracture properties comes from the response times seen at the observation holes. The time required for a pressure transient to propagate through a porous (or fractured) medium is governed by the hydraulic diffusivity (the ratio of permeability to specific storage) of the medium. Higher values of hydraulic diffusivity lead to shorter response times. The observation-hole responses to the C1X05 tests (Figure 7) appeared to be controlled by different rates of change of permeability and specific storage as the pore pressure in the fracture changed during different phases of testing. The post-frac constant-pressure injection test was conducted in two steps, with the first step using a 1-MPa pressure differential and the second step using a 2.3-MPa pressure differential (Figure 3). When the pressure in the fracture was increased during each step, the fracture dilated, increasing its permeability and specific storage. The shorter response times observed during the second step of the post-frac constant-pressure injection test compared to the first step (Figure 7) must reflect an increase in hydraulic diffusivity caused by permeability increasing faster than specific storage. The diffusivity between C1X05 and C1X06 was also higher during the post-frac constant-pressure withdrawal test than during the first step of the injection test. Inasmuch as the flow rate during the withdrawal test was much lower than during the injection test, the increased diffusivity must be related to a decrease in specific storage as the fracture aperture decreased during the fluid withdrawal.

CONCLUSIONS

Two sets of combined permeability and hydraulic-fracturing tests were completed to evaluate how a polyhalitic-anhydrite interbed, MB139, will respond to high gas pressure generated within the WIPP repository. As expected, fracturing took place when the fluid pressure in the interbed exceeded the total local *in situ* stress normal to the fracture plus the tensile strength of the rock. Fracturing at two test locations was associated with horizontal fracture formation primarily along pre-existing, partially or fully healed fractures in the bottom third of the 1-m-thick interbed. Secondary, but greatly subordinate, flow paths appeared to be along closely spaced, tight, subhorizontal fractures in the upper third of MB139. In both cases, fluid was contained along defined stratigraphic horizons. Continued horizontal fracture propagation would limit the maximum pressure in fractures to the overburden pressure.

Fracture development by hydraulic fracturing clearly created new storage capacity because 67% of the hydraulic fracture fluid injected was retained in the formation. Residual fracture apertures after hydraulic fracturing and fracture depressurization to the initial formation pore pressure are estimated to be 0.2 mm. Using a radial hydraulic fracturing model of Geertsma and de Klerk [5], the maximum and average apertures are suggested to be proportional to $R^{1/4}$ where R denotes mean fracture radius.

Some post-frac borehole observations and flow tests suggest that fracturing in MB139 takes place along a strand of fracture branches that extend and become interconnected with time. One of the two hydraulic fracturing tests was initiated near the end of a room where the interbed was relatively undisturbed. However, fracture growth appeared to occur underneath the test room along a path of decreasing (vertical) stress normal to the fluid-induced fracture planes. As a result, the tests described in this study do not resolve the questions whether (1) the stress state in MB139 is isotropic, (2) vertical fracture formation is possible, and (3) fracture extension

could occur along uncertain paths across the nearby anhydrite-rock salt contacts. These questions will be addressed by future measurements in a deeper anhydrite bed.

The pre-and post-frac permeability test of MB139 conducted in test hole C1X10 near a room-drift intersection could not be interpreted using a radial-flow model for homogeneous formations because of apparent variations in fracture aperture, and hence permeability, with distance from the hole. The pre-frac permeability at C1X10 was, however, considerably higher than anticipated, probably because of excavation-related fracturing. The pre-frac permeability of MB139 at the second test hole near the end of the test room was about 10^{-20} m^2.

Hydraulic fracturing clearly resulted in a net increase in permeability and specific storage of MB139 over pre-test conditions at the two test locations. Both properties exhibited a strong pressure-dependence caused by variations in fracture aperture as a function of fluid pressure in the fracture. The permeabilities and specific storage remained higher than pre-frac conditions even when pore pressures were reduced during withdrawal tests, presumably because of incomplete fracture closure as manifested by the high retention of fracture fluid at the end of hydraulic-fracturing tests.

The hydraulic-fracturing tests in Room C1 provided considerable insight into the details of pressure-induced fracturing, the relationship between fracturing and the structure of MB139, and the effects of fracturing on fluid flow and storage capacity. However, neither test was carried out in virgin ground. Although the stress state at the location of C1X05 appeared to approach the undisturbed *in situ* stress state at the repository depth, the hydraulically induced fractures must have advanced asymmetrically toward the room entrance, along the path of decreasing vertical stress under the room floor. The nature of the virgin stress state in MB139, therefore, has not been demonstrated. If it were isotropic, fracturing would be controlled by pre-existing weakness planes, which are subhorizontal. In principle, an anistropic stress state with vertical and horizontal stress differences greater than 2 MPa would allow the development of vertical fractures with uncertain fracture paths.

REFERENCES

1. Borns D.J. *Marker Bed 139: a study of drillcore from a systematic array.* SAND85-0023. Sandia National Laboratories, Albuquerque, New Mexico (1985).
2. Argüello J.G. *Pretest 3-D finite element analysis of the WIPP intermediate-scale borehole test.* SAND90-2055. Sandia National Laboratories, Albuquerque, New Mexico (1990).
3. Wawersik W.R. and Stone C.M. A characterization of pressure records in inelastic rock demonstrated by hydraulic fracturing measurements in salt. *Int. J. Rock Mech. Min. Sci. & Geomech. Abstr.* **26**, 613-627 (1989).
4. Doe T.W. Fractional dimension analysis of constant-pressure well tests. *Proceedings 1991 SPE Annual Technical Conference and Exhibition, Ω Formation Evaluation & Reservoir Geology*, 461-467 (1991).
5. Geertsma J. and de Klerk F. A rapid method of predicting width and extent of hydraulically induced fractures. *J. Pet. Tech.* **21**, 1571-1581 (1969).

Table 1. Selected hydraulic-fracturing data (pressures in MPa). P_0 = pore pressure; P_{b1} = primary (first) breakdown pressure; P_{c1} = fracture extension pressure, first cycle; P_{s1} = first instantaneous shut-in pressure; P_{b4} = breakdown/reopening pressure, fourth cycle; etc.

Borehole	P_0	P_{b1}	P_{c1}	P_{s1}	P_{b4}	P_{c4}	P_{s4}
C1X10	7.4	11.6	10.2	9.7	--	--	--
C1X05	9.6	19.0	n/a	13.8	13.7	12.6	12.4

Figure 1. Healed fractures in lower third of MB139.

Figure 2. Locations of test holes in Room C1.

Figure 3. Experimental sequence in test hole C1X05.

Figure 4. Simulated effects of hydraulic fracturing on fluid production from a constant-pressure flow test.

Figure 5. Pressure records from first and second pressure cycles in test hole C1X05. P_{b1}, P_{b2} = breakdown pressures, first and second cycles; P_{s1}, P_{s2} = instantaneous shut-in pressures.

Figure 6. Flow rates observed during pre- and post-frac constant-pressure flow tests. Offset in C1X10 pre-frac injection data caused by reduction in driving pressure differential.

Figure 7. Response times at observation holes to pressure changes at test hole C1X05.

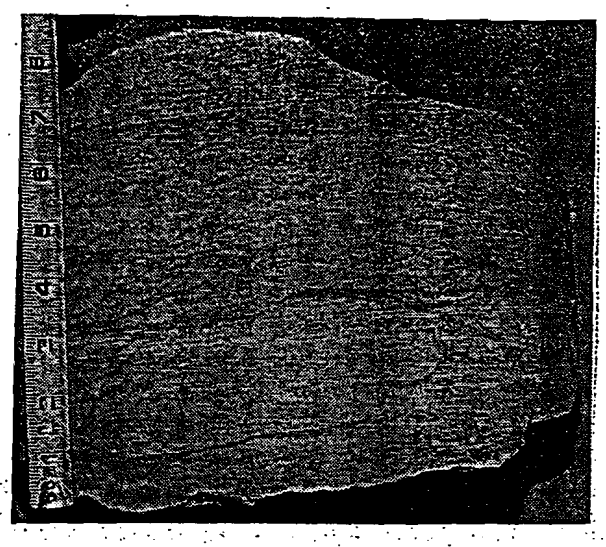

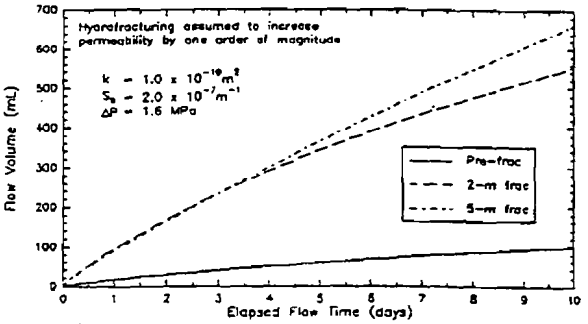
Hydrofracturing assumed to increase permeability by one order of magnitude
k = 1.0 x 10^-19 m^2
S_s = 2.0 x 10^-7 m^-1
ΔP = 1.6 MPa
Pre-frac
2-m frac
5-m frac
Flow Volume (mL)
Elapsed Flow Time (days)

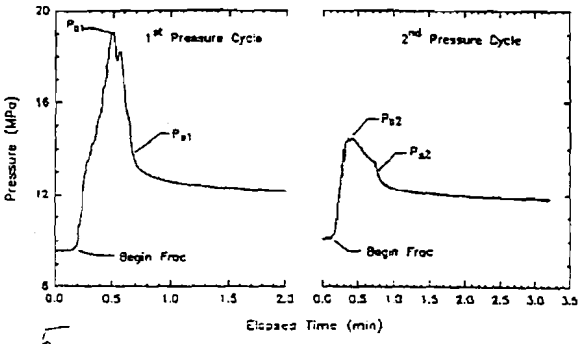
1st Pressure Cycle
2nd Pressure Cycle
Begin Frac
Begin Frac
Pressure (MPa)
Elapsed Time (min)

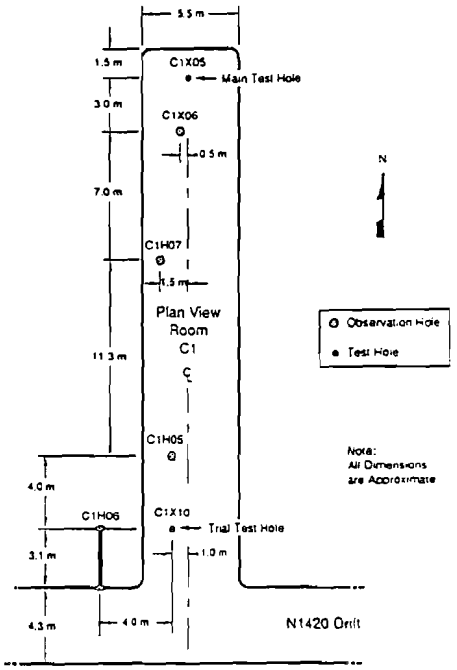
5.5 m
C1X05
Main Test Hole
C1X06
C1H07
Plan View
Room
C1
C1H05
C1H06
C1X10
Trial Test Hole
N1420 Drift
Observation Hole
Test Hole
Note:
All Dimensions
are Approximate
N

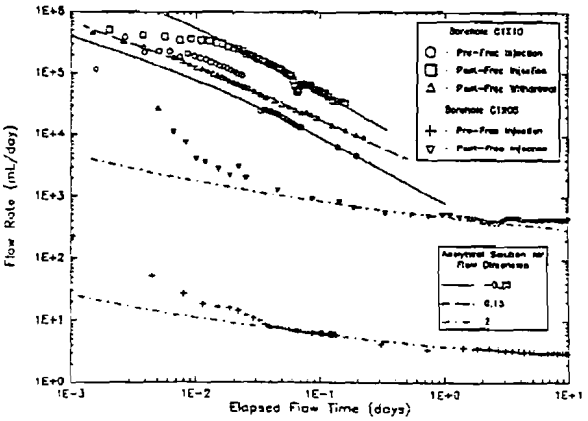
Borehole C1X10
Pre-frac Injection
Post-frac Injection
Post-frac Withdrawal
Borehole C1X05
Pre-frac Injection
Post-frac Injection
Flow Rate (mL/day)
Elapsed Flow Time (days)

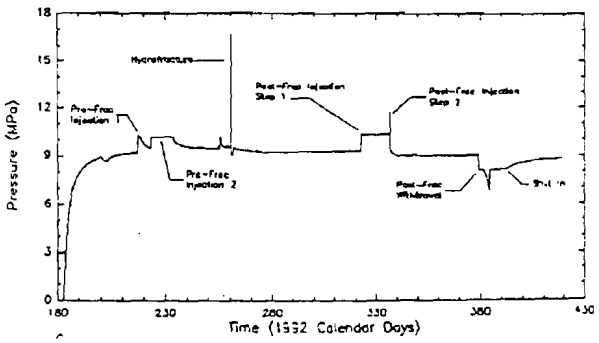
Hydrofracture
Pre-frac Injection 1
Pre-frac Injection 2
Post-frac Injection Step 1
Post-frac Injection Step 2
Post-frac Withdrawal
Shut In
Pressure (MPa)
Time (1992 Calendar Days)

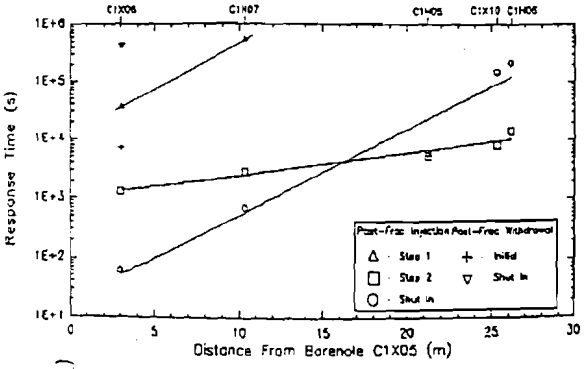
C1X06
C1H07
C1H05
C1X10
C1H06
Post-frac Injection
Post-frac Withdrawal
Step 1
Step 2
Shut In
Initial
Shut In
Response Time (s)
Distance From Borehole C1X05 (m)